ISSN 1063-7710, Acoustical Physics, 2017, Vol. 63, No. 6, pp. 652–659. © Pleiades Publishing, Ltd., 2017.
Original Russian Text © A.I. Belov, G.N. Kuznetsov, 2017, published in Akusticheskii Zhurnal, 2017, Vol. 63, No. 6, pp. 614–622.

OCEAN ACOUSTICS.
HYDROACOUSTICS

Spatial Attenuation of Different Sound Field Components in a Water Layer and Shallow-Water Sediments

A. I. Belov and G. N. Kuznetsov*

Wave Research Center, Prokhorov General Physics Institute, Russian Academy of Sciences, ul. Vavilova 38, 119991 Russia
**e-mail: skbmortex@mail.ru*

Received October 8, 2016

Abstract—The paper presents the results of an experimental study of spatial attenuation of low-frequency vector-scalar sound fields in shallow water. The experiments employed a towed pneumatic cannon and spatially separated four-component vector-scalar receiver modules. Narrowband analysis of received signals made it possible to estimate the attenuation coefficients of the first three modes in the frequency of range of 26–182 Hz and calculate the frequency dependences of the sound absorption coefficients in the upper part of bottom sediments. We analyze the experimental and calculated (using acoustic calibration of the waveguide) laws of the drop in sound pressure and orthogonal vector projections of the oscillation velocity. It is shown that the vertical projection of the oscillation velocity vector decreases significantly faster than the sound pressure field.

*Keywords:*shallow water, low frequencies, sound-signal and mode attenuation in the water layer and bottom, scalar and vector fields

DOI: 10.1134/S1063771017050037

1. INTRODUCTION: EXPERIMENTAL CONDITIONS

The spatial attenuation of sound is an important factor for estimating the efficiency of underwater observations, as well as when organizing acoustic-signal-based navigation and acoustic monitoring systems for a maritime water area. This is especially important for oceanic shelf zones in which the values of the attenuation coefficient for sound signals vary within significant limits depending on the area where experiments are conducted [1]. One of the reasons for the large scatter of sound attenuation is the substantial spatial variability of the acoustic properties of bottom sediments [2, 3]. It should be noted that nearly the entire body of experimental data was obtained earlier using sound pressure (scalar) receivers. Recently, interest has arisen in studying the vector characteristics of acoustic fields, such as the oscillation velocity, oscillation acceleration, or power flow. This is because these characteristics yield additional information on the structure of sound fields and can be used effectively in practical problems [4–6]. Therefore, the study of spatial attenuation of not only the sound pressure (SP) but also the orthogonal projections of the oscillation acceleration vector (OAV) or oscillation velocity vector (OVV) is topical. Note that, to a certain degree, these are conditional "vector" components, because they are calculated with the scalar potential.

Experiments to study the peculiarities in the formation of vector-scalar sound fields have been conducted in a shallow-water area with a depth h_w of 53 m and a sufficiently even bottom. According to geological data, the upper part of the sea bottom was sandy-clayey sediment with a predominant sand fraction. The sound velocity in the water layer decreased from a value of 1477.2 m/s at the surface to 1473.4 m/s at a depth of around 10 m. With depth, the sound velocity slowly increased to a value of 1474.4 m/s at the bottom.

A towed four-component pneumatic cannon was used as a sound source, which was towed at a depth of around 10 m. The depth was recorded. Figures 1a and 1b show the shape and the spectrum of the emitted signal received by a control hydrophone at a distance of 2 m from the source. The emitted pulses were recorded on board a vessel in the unified time system.

Clearly, the structure of the emitted pulse is determined by the shock wave and subsequent gas bubble pulsations. The arrival of a surface-reflected signal lagging 0.0143 s behind the shock wave is also observed. Such a lag is evidence that this pulse was emitted at a depth of approximately 10.5 m. Gas bubble pulsations lead to the appearance of local maxima in the emitted signal spectrum at frequencies $f = 26$, 52, 78, 104, and 130 Hz. At higher frequencies, the maxima in the spectrum are blurred and a monotonic drop in spectral density is observed.

Acoustic signals were recorded by two four-component vector-scalar receiver modules, one of which was near the bottom and the other was raised 22 m above the bottom. The recorded signals were transmit-

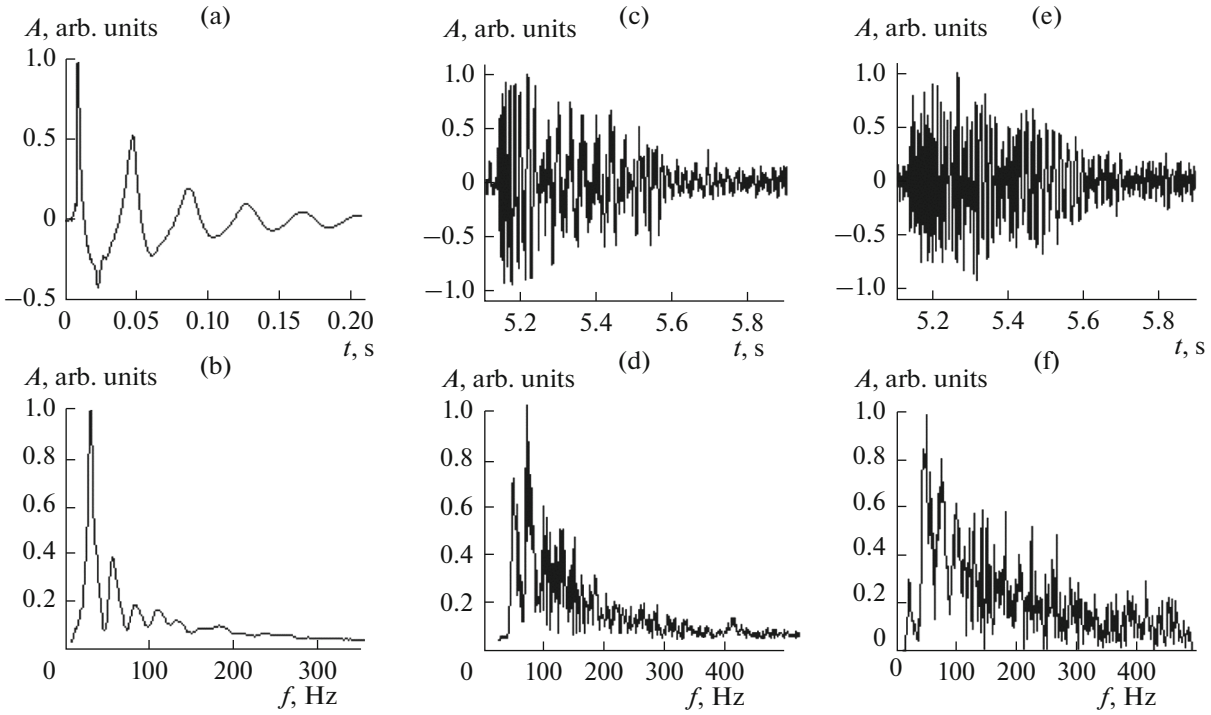

Fig. 1. Time dependences and amplitude spectra of emitted and received pulse signals: (a, b) sound pressure of emitted signal; (c, d) sound pressure; (e, f) vertical oscillation acceleration component of received signal.

ted in digital form via cable to the receiving vessel. The receiving and emitting vessels were equipped with GPS receivers, which made it possible to synchronize the emission and reception modes, measure the coordinates of the receiving and emitting vessels, and calculate the absolute propagation time of pulses. Figures 1c–1f show the time dependences and spectra of the SP and vertical projection of the OAV (VP OAV) received by the upper module at a distance of approximately 7570 m from the emitter.

As vector receivers, we used inertial-type receivers, which recorded three orthogonal oscillation acceleration projections.

From comparison of Figs. 1a, 1b, and 1c–1f, it follows that during propagation, the low-frequency part of the signal significantly weakens much more than the high-frequency part. This effect is especially manifested in the spectra of the vertical component of the oscillation acceleration. The horizontal projection of the OAV (HP OAV) in Fig. 1 is not shown, because at large distances, its structure almost completely coincides with the SP structure [6, 7].

2. EXPERIMENTAL STUDY OF VECTOR-SCALAR FIELD ATTENUATION IN A WAVEGUIDE

2.1. Frequency Dependences of Attenuation of SP and Orthogonal Projections of OAV in a Waveguide

It is of interest to study the laws of attenuation of isolated normal waves propagating in a waveguide and compare the characteristics of attenuation of the SP and orthogonal projections of the OAV. The data are subsequently used to predict sound attenuation in the surface layers of the bottom.

The following procedure was used to estimate the spatial attenuation coefficients for scalar and vector sound fields.

In all recorded realizations of the sound field, 2-s realizations were isolated so that the first second contained only noise, and the second second, noise and pulses of signals emitted within 5 to 10 km to the sound source. Then, in the one-third octave bands with different central frequencies for the time interval of the first second, the noise energy was calculated, and for the second, the noise and signal energy. Here, in the low-frequency region, the central frequencies of the filters corresponded to the positions of local maxima in the spectrum of the signal emitted by the pneumatic cannon (see Fig. 1). After this, signal energy estimates were obtained from the energy of the sum of the signal and noise. The distance dependences of the signal energy were approximated by the cylindrical law of the drop in pulse with additional exponential attenuation. Analysis of the results showed that the additional attenuation b is almost identical for the SP and HP OAV, and for the VP OAV, it can be appreciably higher. The frequency dependences of the b value for the two reception depths are shown in Fig. 2.

Clearly, in the case of near-bottom reception, the VP OAV attenuation coefficients exceed the SP attenuation coefficients in nearly the entire frequency

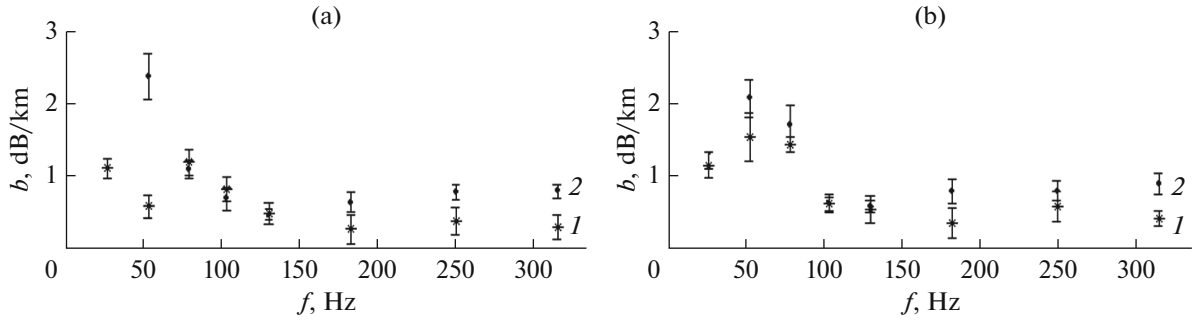

Fig. 2. Frequency dependences of spatial attenuation coefficients: (a) raised module, (b) bottom module. (*1*) pressure, (*2*) vertical projection of oscillation acceleration.

range. For the raised module, this effect is observed at 100–150 Hz or higher.

2.2. Study of the Laws of Attenuation of Normal Waves

For subsequent analysis, narrowband filtering of the recorded signals was done to select the modes forming the received signals. The width of the filter at each frequency was chosen to best estimate the arrival time of each mode. Figure 3 shows the results of such filtering for the raised modulus. The distance from the emission point was approximately 7575 m.

It has been established that at frequencies higher that 30 Hz, the time structure of the signals recorded by the SP and OAV receivers are different. Whereas the SP field is mainly formed by the first and third modes, in the VP OAV field, the main role is played by the second mode. This completely corresponds to the results of [7, 8] and is related to the position of the raised module near the zero of the second SP mode, whereas at the same depth, the second mode of the VP OAV reaches the maximum value. At 26 Hz, in a waveguide at large distances there is only one mode in the sound field, the first. The remaining modes at such a distance have already almost completely attenuated. Therefore, the acoustic field attenuation coefficients at this frequency are the same for both receiver modules (see Figs. 2, 3). At 180 Hz, the signal recorded by the VP OAV receiver component is appreciably longer than the signal received by the SP receiver. This testifies to the fact that at this frequency, in the formation of the VP OAV field, a significant role is played by higher-number modes, the contribution of which to the SP field is insignificant [8]. Therefore, at higher frequencies, the VP OAV attenuation components are noticeably larger than the pressure attenuation coefficients, since during multimode sound propagation, in the formation of the VP OAV, lower-number modes having, as a rule, the minimum attenuation coefficients are suppressed, whereas higher-number modes are emphasized. It can also be seen that at 52 Hz, a second mode can be traced in the SP signal, which at higher frequencies is practically undetectable. In [9] it was shown that with a decrease in frequency, the positions of the minima and maxima of the mode amplitude shift toward the sea bottom, and this shift is the larger, the lower the frequency. Therefore, manifestation of the second mode in the structure of a pressure pulse at 52 Hz is caused by the shift of the zero of this mode with respect to the depth of the raised module. On this basis, the authors of [10] proposed using the location depths of zeros and maxima of the vertical distribution of modes to estimate the sound velocity in the upper part of bottom sediments.

To estimate the attenuation coefficients for individual modes, narrowband filtering of received signals was done at different distances to the emitter. Here, the location of the vector-scalar module manifested itself predominantly near the zero of the second mode. Figure 4 shows the structure of a pulse signal at 104 Hz for the two receiver modules and three distances from the sound source. From the figure it follows that for the raised module, at all chosen distances, three modes are resolved, whereas for the bottom module, mode selection is possible only at the maximum distance. Therefore, below, the attenuation coefficients of the first three modes are estimated from the signals of the raised module.

To estimate the attenuation coefficients in the chosen frequency bands, the envelopes of all signals were isolated. Then, the time intervals were established in which the values of the envelop of each mode were equal to or exceeded half its maximum value. This was done, on the one hand, to maximally exclude the influence of neighboring modes at higher frequencies, and on the other hand, to take into account intramode dispersion. In each time interval, the energy of the corresponding mode was calculated at different distances. The dependence of the mode energy on distance was corrected to the cylindrical law of divergence, after which, the spatial coefficient of mode attenuation g_m was estimated by the least squares method. Figure 5 shows the frequency dependences of the attenuation coefficients of the first three modes.

The estimates of the mode attenuation coefficients B were the basis for determining the absorbing proper-

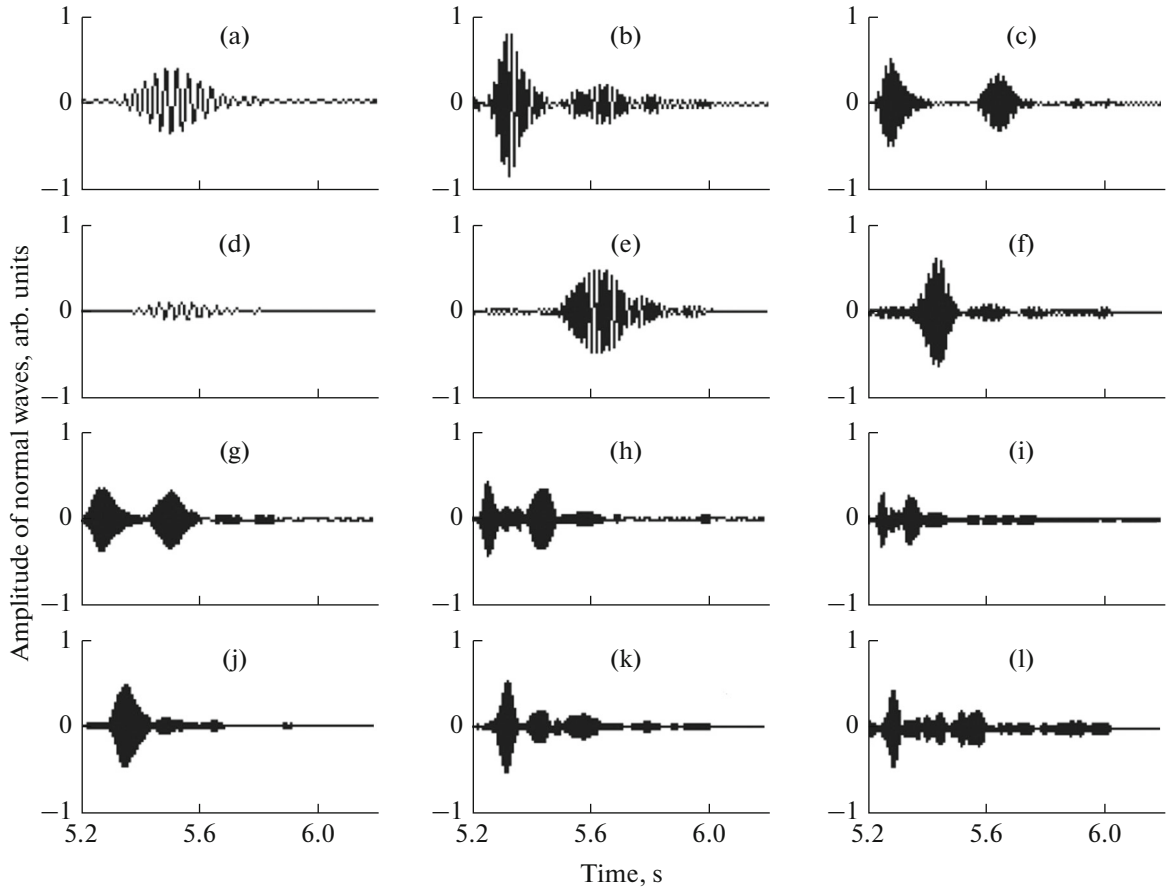

Fig. 3. Results of narrowband filtering of received signal (a–c), (g–i) pressure; (d–f), (j–l) vertical component of oscillation acceleration. Frequency f: (a, d) 26; (b, e) 52; (c, d) 78; (g, j) 104; (h, k) 130; (i, l) 180 Hz.

ties of the sea bottom. Here, the results of [8] were used, in which from the same experimental data a bottom model was obtained in the form of a fluid layer with a thickness of $h_L = 18.9$ m, lying on a halfspace; the density and sound velocity values in this layer and the halfspace were also estimated. It was established that for the characteristics at frequencies higher than 50 Hz, it is possible to ignore the influence of the halfspace on the sound field in the water layer at large distances. Therefore, this study used the results obtained at frequencies higher than 50 Hz, and the sea bottom was considered as a halfspace with the following parameters of the upper layer of the bottom: density ρ 1467 kg/m^3 and sound velocity c 1634.4 m/s. In such a model, the absorbing properties of the bottom are characterized by the parameter α, which is responsible for the imaginary part of the wavenumber in the bottom, which in turn is given as $\tilde{k} = k(1 + i\alpha)$, $k = 2\pi f/c$ [2, 3].

These characteristics of the model were sought in the same way as in [11], by minimizing the functional of the form

$$L = \sum_{f_g} \sum_{n_g} (g^e - g^c)^2 \sigma_g^{-2}, \qquad (1)$$

where σ_B is the mean square deviation of the experimental estimates for the mode attenuation coefficients; f_g, n_g are the frequency values and mode numbers at the frequencies for which estimates of the attenuation coefficients were obtained. The superscripts e and c denote, respectively, the experimental estimates and calculated values of the mode attenuation coefficients. Functional (1) was minimized by the Nelder–Mead multidimensional optimization method (simplex method) [12].

For successful optimization as a result of nonlinearity of the algorithm, it is desirable to set the initial values of the these parameters close the sought ones. The initial values of the parameters were found as follows. The water layer was replaced by an isovelocity layer with a sound velocity of $c_w = 1475$ m/s. For such a waveguide model (Pekeris waveguide), the authors of [3] gave the initial expressions with which it is possible to obtain the formulas that relate in explicit form the sought parameter α and the mode attenuation coefficients g_m:

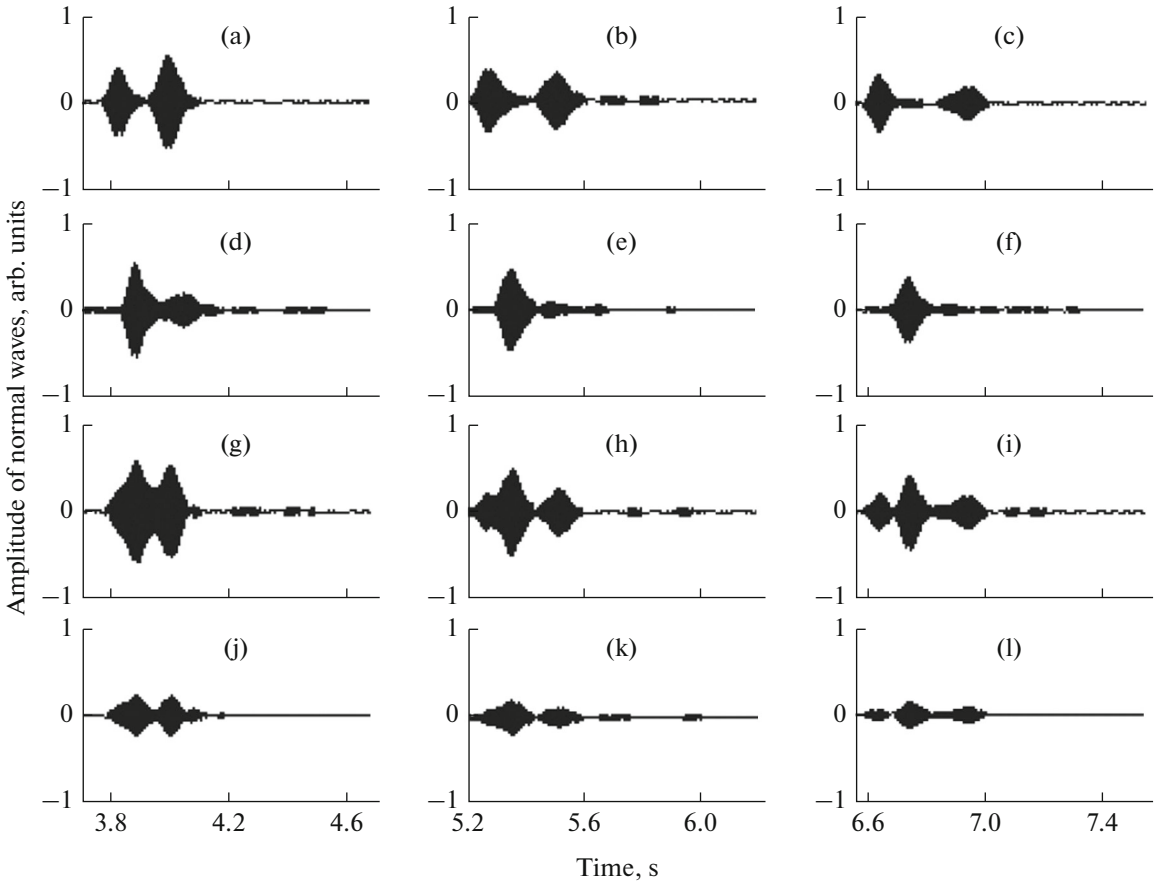

Fig. 4. Structure of pulse signals at frequency of 104 Hz: (a–f) raised module; (g–l) bottom module. (a–c), (g–i) pressure; (d–f), (j–l) vertical projection of oscillation acceleration; (a, d, g, j) $r = 5475$; (b, e, h, k) $r = 7570$; (c, f, i, l) $r = 9505$ m.

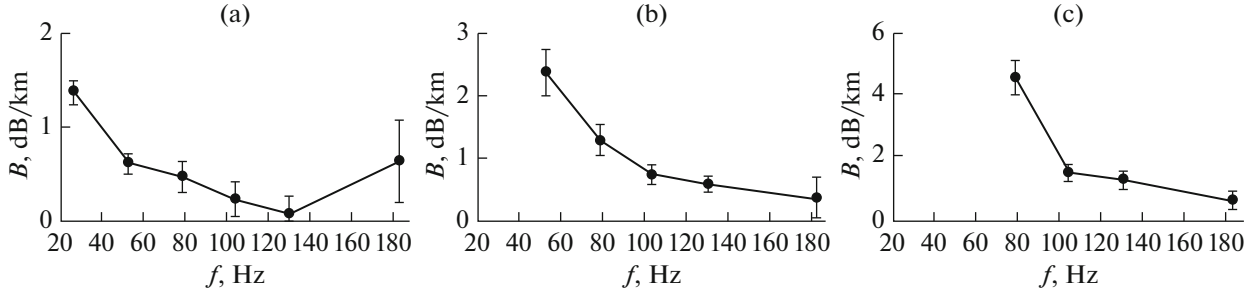

Fig. 5. Attenuation coefficient of first three modes: (a) mode 1, (b) mode 2, (c) mode 3.

$$\alpha = 2g_m\xi_m\gamma N\frac{\gamma^2 + d^2\gamma_w^2}{\gamma_w^2\gamma^2 d},\quad N = \frac{h_w}{2} + \frac{d}{2\gamma\gamma^2 + d^2\gamma_w^2}\frac{k_w^2 - k^2}{},\quad (2)$$
$$\gamma_w = \sqrt{k_w^2 - \xi_m^2},\quad \gamma = \sqrt{\xi_m^2 - k^2},\quad d = \rho/\rho_w,$$
$$k_w = 2\pi f/c_w,$$

where m is the mode number. Water density ρ_w is considered to be 1000 kg/m^3. The longitudinal wavenumbers of modes ξ_m were estimated for the ideal waveguide model with perfectly soft boundaries and an effective water layer width of $H = h_w + \Delta h$. In accordance with [13], quantity Δh is determined as $\Delta h = d(k_w \sin\theta)^{-1}$, $\theta = \arccos(c_w/c)$. For such a model, longitudinal wavenumbers ξ_m are determined by the well-known formula $\xi_m = \sqrt{k_w^2 - (\pi m/H)^2}$. Such an approximation yields quite good accuracy for modes whose phase velocity noticeably exceeds the sound velocity in the halfspace.

Table 1. Dependence of parameter α on frequency

Frequency, Hz	78	104	130	180
α	0.0084 ± 0.0016	0.0093 ± 0.0015	0.0082 ± 0.002	0.0087 ± 0.0065

The initial approximation of parameter α was estimated from the experimentally measured frequency dependence of the attenuation coefficient of the second mode, because it best corresponds to the theoretically representations in a wide frequency band. The table 1 gives the α estimates for four frequencies.

To minimize functional L for all frequencies, a mean value of $\alpha = 0.0086$ was taken as the initial approximation. This is based on the data in the table 1, from which follows a weak dependence of α on frequency. This indirectly confirms the possibility of describing the fields at these frequencies with the Pekeris–Brehovsky model, because for this model, α is given as a constant value for all modes and frequencies [14, 15].

As a result of this numerical optimization using (1) and (2), a value of $\alpha = 0.0072$ was obtained. Figure 6 compares the experimental data and calculated attenuation coefficients of the first three modes for two α equal to the calculated 0.0072 and the 0.0086 taken directly from experiment. Despite the fact that the value of α was sought for the experimental data at frequencies higher than 50 Hz, Fig. 6 shows all available experimental data, including for lower frequencies.

Clearly, for an appreciable difference in the two α values, their use approximates the experimental data with sufficient accuracy. To explain this effect, the error in estimating α was calculated using formula (3) [16]:

$$\sigma_\alpha = \left[s^2 \left(\frac{1}{2} \frac{\partial^2 L}{\partial \alpha^2} \right)^{-1} \right]^{1/2}, \qquad (3)$$

in which the second derivatives of parameter α are calculated at the point where the L value reaches the minimum $L_{\min}$. Quantity s^2 is found from the scatter of the g^e values with respect to the theoretical $s^2 = \left[\sum_n \sum_f (g^e - g^c)^2 \right] \Big/ \left(\sum m - 1 \right)$ curves, where m is the total value of the estimates for the mode attenuation coefficients [14]. It turned out that the size of the error σ_α has quite a large value: 0.0063. This may why appreciable differences in the α value do not lead to substantial divergences of the approximating curves.

3. COMPARISON OF THE DEPENDENCES OF THE VECTOR-SCALAR FIELDS WITH THE CHARACTERISTICS CALCULATED AS A RESULT OF WAVEGUIDE CALIBRATION

Analysis of the aforementioned experimental data characterizing the laws of the drop in the scalar and vector components is of certain practical interest. However, to predict both the SP and OP OAV fields, an adequate experimentally confirmed waveguide model is needed. Today, most authors use the flat-layered waveguide model with a lower boundary (the bottom) given in the form of a fluid or an elastic halfspace. The bases of the model were laid in [14, 15] and developed, e.g., in [3]. In [9], a model of the transfer function of a waveguide with a flat-layered bottom was developed. We also use as the bottom model a system of fluid layers lying on a hard or fluid halfspace (this study and, e.g., [6–8, 11]. However, in this case, for predictive calculations, the results of experimental estimation of the characteristics of these layers and the halfspace are needed. In [8], the waveguide was acoustically calibrated and the mentioned characteristics were calculated experimentally for the studied area. This made it possible to construct the model of the waveguide transfer function and compare the experimentally measured and calculated dependences of the SP and OP OAV values. It is assumed that the developed model is confirmed (or refuted) in the case of agreement (or disagreement) of these dependences.

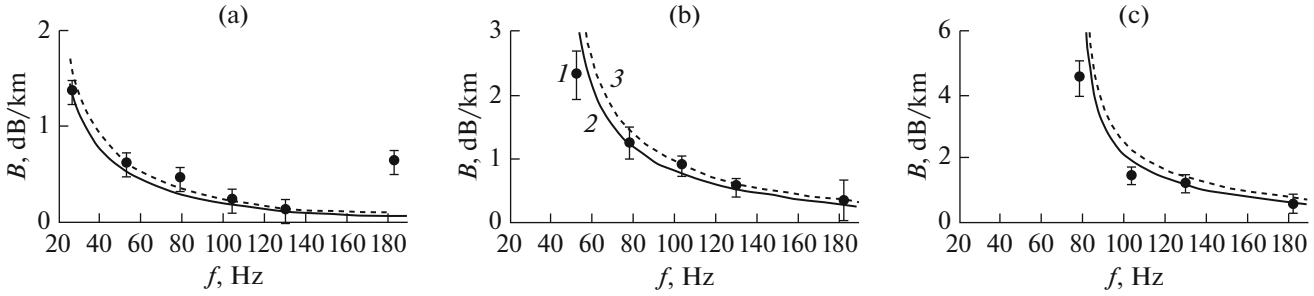

Fig. 6. Frequency dependences of attenuation coefficients of first three modes: (a) mode 1, (b) mode 2, (c) mode 3; (*1*) experimental data, (*2*) calculated for $\alpha = 0.0072$, (*3*) calculated for $\alpha = 0.0086$ (solid and dotted lines, respectively).

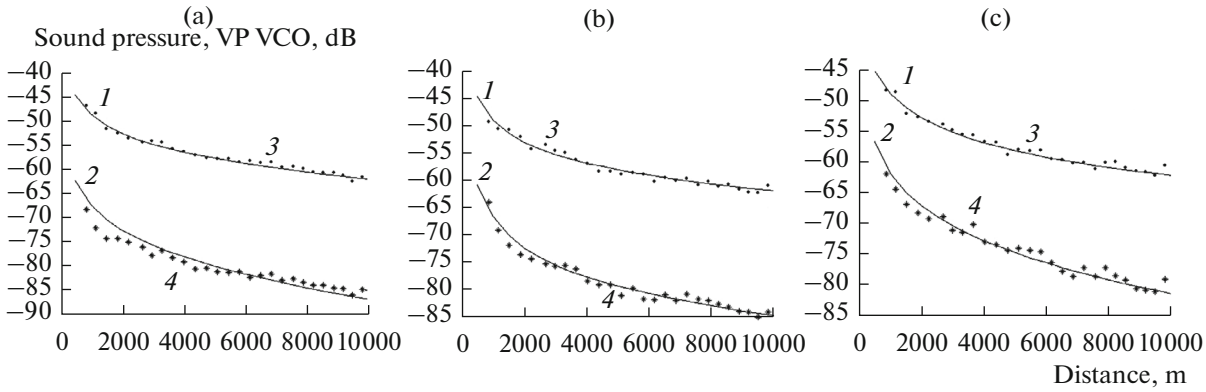

Fig. 7. Comparison of calculated (*1*, *2*) and measured (*3*, *4*) dependences of SP and vertical component of oscillation acceleration on distance: *1*, *3*—pressure; *2*, *4*—oscillation acceleration; (a, b, c) frequencies of 130, 183, and 315 Hz, respectively.

We have compared the measured spatial attenuation values of the vector-scalar field components values and those calculated with the developed bottom model at relatively high frequencies [8]. The reason is that for small-mode propagation, random depths of the emission and reception points play an excessively important role, since the relation of the amplitudes of propagating modes substantially depends on the coordinates. Therefore, for the raised module, Fig. 7 compares the spatial dependences of the SP and VP OAV measured experimentally and calculated with the model at frequencies higher than 100 Hz.

It is also interesting to compare to laws of the drop in the SP and VP OAV at frequencies not taken into account when developing the model. For this, Fig. 7c compares the experimental and calculated data at a frequency of 315 Hz. Clearly, at all frequencies, the experimental dependences of both the SP and the VP OAV agree well with the characteristics calculated with the multilayer waveguide model constructed as a result of acoustic calibration. Here, the VP OAV also constructed with higher-number modes attenuates more quickly than the SP and HP OAV.

It is also clear that in individual areas of the distance dependences, deviations of the experimental data from the calculated data are observed. Essentially, these deviations at different frequencies are manifested in the same distance intervals; i.e., they are not random. From the comparison of the deviations for the SP and VP OAV values (see Fig. 7), it can be concluded that the main factor is not variation in the waveguide depth along the towing track, but the corresponding variation in the bottom characteristics, due to which larger deviations are observed in the VP OAV dependence in comparison with the SP.

4. CONCLUSIONS

A waveguide in which oscillation accelerations (or velocities) form is a spatial filter that "weighs" its horizontal and vertical projects differently. HP OAVs suppress higher-number modes, and VP OAVs suppress modes of the first numbers.

The attenuation coefficient of the VP OAVs at middle and high frequencies exceeds by a factor of 2 or more the attenuation coefficient of scalar signals and HP OAVs. With an increase in distance, at low frequencies for a small number of modes, within the limit—during propagation of one mode—the values of the attenuation coefficients are close to each other. As a result, the attenuation coefficients at the lowest frequencies become close to each other.

Owing to the difference in the spatial filtering of different mode numbers, in the time domain, different wave packets are formed at the outputs of the SP, VP OAV, and HP OAV receivers, which is important for their active ranging. In particular, at the output of the vertical channels, the signals are notably "drawn out" in comparison to the remaining channels. The attenuation coefficients of individual modes significantly (twofold or more) increase with increasing mode number.

The proportionality coefficient in front of the imaginary part of the wavenumber, which characterizes the value of sound signal attenuation in bottom sediments, depends weakly on frequency and can be taken as a constant, which agrees with the Pekeris–Brehovsky model and indirectly confirms its possible use at least at middle frequencies.

The laws of attenuation of the OAV and SP components, measured and calculated from the results of acoustic waveguide calibration, agree well with each other, but at different distances, deviations of the experimental dependences from the calculated ones are observed for all frequencies. Since these deviations for the VP OAV significantly exceed the deviations for the SP field (and the HP OAV), we can assume that the reason is variation in the characteristics of the surface layers of the bottom along the emitter towing track.

ACKNOWLEDGMENTS

The authors are obliged to V.G. Petnikov for useful discussion of the paper.

REFERENCES

1. N. V. Studenichnik, Acoust. Phys. **42** (1), 119–123 (1996).
2. N. S. Ageeva and V. D. Krupin, Akust. Zh. **26** (2), 161–166 (1980).
3. B. G. Katsnelson and V. G. Petnikov, *Acoustics of the Shallow Sea* (Nauka, Moscow, 1997) [in Russian].
4. V. A. Shchurov, *Vector Acoustics of the Ocean* (Dal'nauka, Vladivostok, 2003) [in Russian].
5. N. I. Belova and G. N. Kuznetsov, Acoust. Phys. **59** (2), 228–239 (2013).
6. A. I. Belov and G. N. Kuznetsov, Acoust. Phys. **62** (3), 319–327 (2016).
7. A. I. Belov, N. I.Belova, and G. N. Kuznetsov, in Proc. Acad. L. M. Brekhovskikh's 12th School-Seminar "Acoustics of the Ocean" (GEOS, Moscow, 2009), pp. 27–30.
8. A. I. Belov and G. N. Kuznetsov, Acoust. Phys. **62** (2), 194–201 (2016).
9. N. S. Ageeva and V. D. Krupin, Akust. Zh. **27** (5), 669–677 (1981).
10. L. Rubano, J. Acoust. Soc. Am. **67** (5), 1608–1613 (1980).
11. A. I. Belov and G. N. Kuznetsov, Phys. Wave Phenom. **21** (3), 177–182 (2014).
12. J. A. Nelder and R. Mead, Computer J. **7** (4), 308–313 (1965).
13. D. E. Weston, J. Acoust. Soc. Am. **65** (2), 647–654 (1960).
14. K. Pekeris, in *Sound Propagation in the Sea* (InLit, Moscow, 1951), pp. 48–156, [in Russian].
15. L. M. Brekhovskikh, Waves in Layered Media (Akad Nauk, Moscow, 1957), [in Russian].
16. D. J. Hudson, Statistics. Lectures on Elementary Statistics and Probability (Geneva, 1964).

Translated by A. Carpenter